Model of ELM suppression by RMPs in DIII-D*

J.D. Callen,[1] M.T. Beidler,[1] N.M. Ferraro,[2] C.C. Hegna,[1]
R.J. La Haye,[3] R. Nazikian,[2] C. Paz-Soldan[3]

[1]*University of Wisconsin, Madison, WI 53706-1609 USA*
[2]*Princeton Plasma Physics Laboratory, Princeton, NJ 08543-0451 USA*
[3]*General Atomics, San Diego, CA 92186-5608 USA*

Introduction: This paper presents theory-based descriptions of how resonant magnetic perturbation (RMP) effects on the edge magnetic field and pedestal suppress edge localized modes (ELMs) in recent DIII-D experiments [1, 2]. These seminal experiments explored the effects near the minimum applied $n = 2$ RMP amplitude required for ELM suppression in ITER-relevant low collisionality pedestals. They demonstrated that when resonant fields are large enough, an ELM crash in those experiments [1, 2] induces an abrupt bifurcation into a new plasma state that has (Fig. 1): 1) an extra* (red asterisks indicate parts of figures being discussed), externally measured high field side (HFS) $n = 2$ tearing-type poloidal magnetic response $|\delta B_\theta|$, 2) increased* carbon toroidal flow speed V_ϕ at the pedestal top, and 3) slightly reduced* electron density $n_{e,\mathrm{ped}}$, temperature $T_{e,\mathrm{ped}}$.

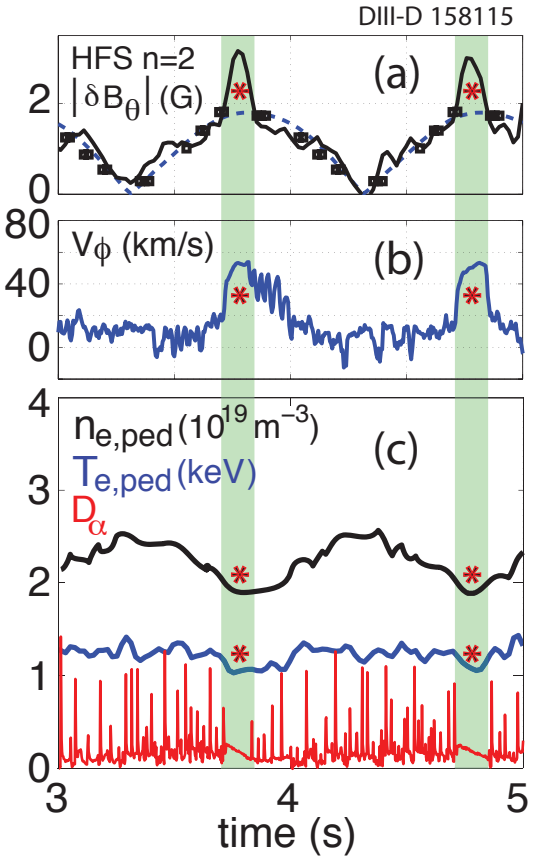

Figure 1: Pedestal parameters vary as upper/lower I-coil phasing changes $|\delta B_\theta|$ slowly in DIII-D [1,2], in (a) from minimum RMP at 3.3 s to maximum RMP at 3.7 s and again from 4.3 and 4.7 s. Shaded vertical bands indicate times where ELM suppression occurs. Red asterisks (*) indicate parts of the figure empasized in the text.

Forced magnetic reconnection (FMR) theory: When 3-D RMPs are applied to an axisymmetric tokamak plasma, two states are possible: one has large flow screening of RMPs at $q = m/n$ rational surfaces with little magnetic reconnection there; the other has small flow at a rational surface and significant RMP field penetration there which induces a tearing-type magnetic response. The original theory [3] for this "Taylor problem" was developed for a sheared magnetic field in a resistive MHD slab model that had no equilibrium plasma flows. Subsequently, cylindrical models with flows were developed for mode-locking induced by 3-D resonant field errors [4] and bifurcations they induce [5], including diamagnetic flow effects [6, 7, 8]. A comprehensive theory which explores the temporal and spatial development of FMR effects that is applicable to the magnetic geometry, low collisionality and parameters in tokamak edge plasmas is being developed [9].

Flow screening before bifurcation: In the ELMing "equilibrium" before bifurcation ($t \lesssim 3.7$, 4.7 s in Fig. 1), strong flow screening by plasma flows occurs at $q(\rho_{m/n}) = m/n$ rational surfaces.

The predicted factor [5, 9] by which the RMP field is reduced from its vacuum value there is $f_{\rm scr} \equiv \frac{B_{mn}(\rho_{m/n})}{B^{\rm vac}_{mn}} \gtrsim \frac{m}{-in\Omega^\alpha_e \tau_\delta}$. Here, $\Omega^\alpha_e \equiv -[\frac{d\Phi_0}{d\psi_{\rm p}} - \frac{1}{n_{e0}e}\frac{dp_{e0}}{d\psi_{\rm p}} - \frac{0.71}{e}\frac{dT_{e0}}{d\psi_{\rm p}}] = \omega_{\perp e} + \frac{0.71}{e}\frac{dT_{e0}}{d\psi_{\rm p}}$ is the rotation frequency of the electron fluid in the "perpendicular" $[\vec{\nabla}\alpha \equiv \vec{\nabla}\phi - (m/n)\vec{\nabla}\theta]$ direction, including T_e gradient effects [9]. The reconnection time is approximated by [5, 9] $\tau_\delta \simeq 2S^{2/3}\tau_A \simeq 14$ ms where $S \equiv \tau_R/\tau_A \simeq 1.3\times10^8$ is the Lundquist number, $\tau_R \equiv \rho^2_{m/n}/D_\eta \simeq 3.7$ s and $\tau_A \equiv L_{\rm sh}/mc_A \simeq 2.8\times10^{-8}$ s ($B_0 \simeq 1.9$ T) are global resistive and shear-Alfvén times (values herein are at the 8/2 rational surface at 4780 ms [2, 10]). The effective magnetic field diffusivity is [9, 10] $D_\eta \equiv \overline{g}^{\rho\rho}\eta^{\rm nc}_\parallel/\mu_0 \simeq 0.14$ m^2/s and magnetic shear length $L_{\rm sh} \equiv R_0 q/\hat{s} \simeq 1.9$ m. For $|\Omega^\alpha_e| \gtrsim 10^4$ rad/s, the predicted screening factor is $f_{\rm scr} \lesssim 0.03$, which yields [10] $B_{mn} \lesssim 0.031$ G/kA (i.e., $B_{mn} \lesssim 0.12$ G for the 4 kA I-coil current [2]). One-fluid (1F) linear numerical modeling by M3D-C1 [11] before bifurcation produces results of a similar magnitude at all rational surfaces. But during the period when ELMs are suppressed, M3D-C1 indicates (Fig. 2) little screening at the 8/2 surface ($f_{\rm scr} \simeq 0.8$).

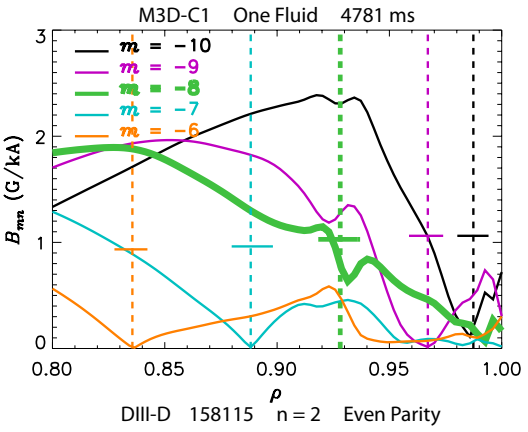

Figure 2: Resonant radial magnetic perturbations [11] in the edge of DIII-D are strongly screened at all rational surfaces, except the 8/2 response at $t = 4781$ ms (during suppression). Horizontal dashes indicate $B^{\rm vac}_{mn}$ values.

Penetration during ELM crash, 4704.6–4706 ms (Fig. 3): The spikes in the D_α signals in Fig. 1 are caused by peeling-ballooning (P-B) ideal MHD instabilities that grow and then decay on a MHD time scale of about 0.4 ms. When RMPs are present, the rest of the ELM crash phase that lasts about 1 ms has the following properties (Fig. 3): 1) an extra* $n = 2$ magnetic perturbation is induced on the HFS of DIII-D with an initial toroidal rotation frequency of about $\Omega_{\rm t} \sim 2\times10^3$ rad/s; and then 2) it transitions into a $n = 2$ wall-locked ($\Omega_{\rm t} \to 0$) tearing-type response that increases the externally measured δB_θ by about 1.2 Gauss over its value before bifurcation (Figs. 1 and 3). At present there is no nonlinear theory or simulation for how an ideal MHD P-B mode produces such an increased $n = 2$ perturbation. However, theory developed for how sawtooth and ELM crashes may seed neoclassical tearing mode (NTM) islands [12] can be used here. That theory predicts [9] the radial component of a resonant MHD perturbation induces magnetic reconnection at the resonant surface that grows rapidly in time up to the inverse of the evolving toroidal rotation frequency, > 0.5 ms here. The tearing-type perturbation at the 8/2 surface induces a magnetic island of width w $\simeq 4\,[(L_{\rm sh}/k_\theta)B_{82}(\rho_{8/2})/B_0]^{1/2}$, in which $k_\theta = m/\rho_{8/2} \simeq 11/$m is the poloidal wavenumber. A magnetic island is relevant because [13] the inferred w/2 here is larger than the reconnection singular width $\delta_\eta \simeq \rho_{m/n}/S^{1/3} \simeq 0.14$ cm.

Toroidal flow during ELM crash: Magnetic reconnection induced by the ELM crash causes a large instantaneous, non-ambipolar "flutter model" [14] radial electron density flux in the δ_η layer at $\rho_{m/n}$ of $\Gamma^{\rm flutt}_e(\rho_{m/n}) = -n_e D_{et}[\frac{d\ln p_{e0}}{d\rho} + 0.71\frac{d\ln T_{e0}}{d\rho} - e\frac{d\Phi_0}{d\rho}] = -n_e D_{et}\frac{eRB_{\rm p}}{T_e}\Omega^\alpha_e$. The flutter diffusivity at $\rho_{8/2} \simeq 0.93$ is [10, 14] $D_{et}(\rho_{8/2}) \simeq 0.3\,(v^2_{Te}/\nu_e)\,[B_{82}(\rho_{8/2})/B_0]^2 \sim 44$ m^2/s [for $B_{82}(\rho_{8/2}) \sim 3.1$ G], in which the electron thermal speed $v_{Te} \equiv (2T_e/m_e)^{1/2} \simeq 2\times10^7$ m/s and

electron collision rate $\nu_e \simeq 7.4\times10^4/\mathrm{s}$. This non-ambipolar electron flux induces a toroidal torque density $T_\phi^{\mathrm{flutt}} = RB_\mathrm{p} e\Gamma_e^{\mathrm{flutt}}$ that is usually in the co-current direction at the pedestal top. Ambipolarity is preserved by a rapid increase in the radial electric field $E_\rho \equiv -d\Phi_0/d\rho$ from a large negative value up to where $\Omega_e^\alpha \simeq 0$ so $\Gamma_e^{\mathrm{flutt}}(\rho_{8/2}) \simeq 0$ and $T_\phi^{\mathrm{flutt}}(\rho_{8/2}) \simeq 0$ [14, 10]. Figure 3 shows that for the largest RMP this causes the carbon (C) toroidal flow speed $V_\phi \simeq [E_\rho - (1/6n_C e)dp_{C0}/d\rho]/B_\mathrm{p}$ after 4707 ms to increase** from near zero by about 20 km/s — as $\delta\mathrm{B}_\theta$ evolves during* and beyond** the initial tearing stage. It also apparently causes the plasma toroidal rotation at the 8/2 rational surface to "lock into" the RMP laboratory frame (i.e., $\Omega_\mathrm{t} \simeq \Omega_E^\alpha \equiv -d\Phi_0/d\psi_\mathrm{p} = E_\rho/RB_\mathrm{p} \simeq 0$) in the δ_η layer, because flutter transport quickly relaxes the n_e and T_e gradients there. High temporal resolution studies of similar ELM crashes in DIII-D [15, 16] have shown pedestal n_e, T_e and flow gradients decrease significantly during this $\delta t \sim 1$ ms stage.

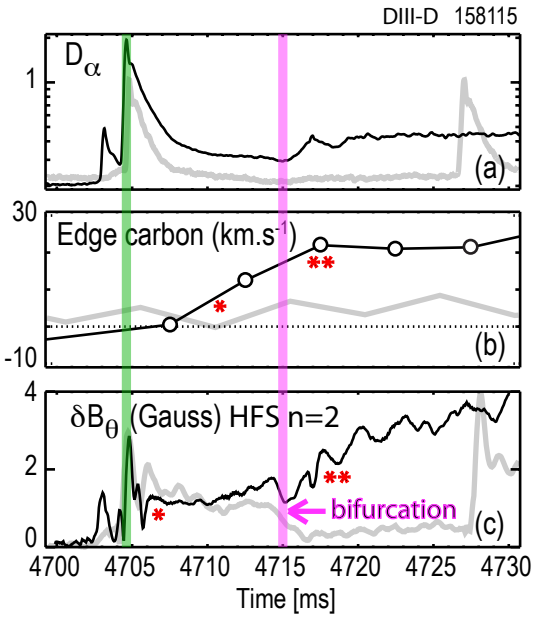

Figure 3: Short time scale dynamics of D_α, carbon toroidal flow and extra* HFS magnetic perturbation around ELM crash at 4704.6 that bifurcates into ELM suppressed state after 4715 for largest RMP. Gray lines for smallest RMP are shifted for ELMs at 4307 and 4330.

Initial tearing stage, 4706–4715 ms: Just after the ELM crash: 1) flutter transport [14] is predicted to radially diffuse initially localized n_e, T_e, V_ϕ responses away from the $\delta_\eta \simeq 0.14$ cm layer in a time $\tau_\mathrm{spread} \sim (\Delta\rho)^2/D_{et}(\rho_\mathrm{mid}) \sim 0.25 \to 4$ ms for $\Delta\rho \sim 1 \to 4$ cm in which [14, 10] $D_{et}(\rho_\mathrm{mid}) \simeq (\nu_e \mathrm{v}_{Te})^{1/2}(R_0 q)^{3/2}[B_{mn}(\rho_\mathrm{mid})/B_0]^2 \simeq 0.4\ \mathrm{m}^2/\mathrm{s}$ [for $B_{mn}(\rho_\mathrm{mid}) \sim 2.4$ G at the mid-point $\rho_\mathrm{mid} \simeq 0.95$ between the 8/2 and 9/2 surfaces]; 2) poloidal flow is damped to its neoclassical equilibrium in $\tau_{ii} \sim 3$ ms, and 3) the ballooning-type low field side (LFS) $n = 2$ magnetic perturbation [1] decays in about 5 ms. But the extra* HFS-measured $n = 2$, $\Omega_\mathrm{t} \simeq 0$ $\delta\mathrm{B}_\theta$ perturbation is about constant during this stage (see Fig. 3) for both the smallest and largest RMPs.

Bifurcation after 4715 ms: The response to an ELM crash is nearly independent of the applied RMP amplitude up to this time. Further temporal evolution of $\delta\mathrm{B}_\theta \sim B_{82}(\rho_{8/2}) \propto \mathrm{w}^2$ is governed by (because $\mathrm{w} \gg 2\delta_\eta \simeq 0.3$ cm) the nonlinear, modified Rutherford [13, 9] equation:

$$\frac{d\mathrm{w}}{dt} \simeq D_\eta \left[\Delta'_{8/2} + \Delta'_{\mathrm{RMP}} \frac{\mathrm{w}_{\mathrm{vac}}^2}{\mathrm{w}^2} - \frac{\mathrm{w}_{\mathrm{pol}}^3}{\rho_{8/2}\mathrm{w}^3}\right], \quad \mathrm{w}_{\mathrm{vac}} \equiv 4\left[\frac{L_{\mathrm{sh}}}{k_\theta}\frac{B_{82}^{\mathrm{vac}}(\rho_{8/2})}{B_0}\right]^{1/2} \simeq 2.4\ \mathrm{cm}. \quad (1)$$

Here, NTM effects and order unity numerical factors have been neglected. Also, $\Delta'_{8/2} \simeq -2k_\theta \simeq -22/\mathrm{m}$, $\Delta'_{\mathrm{RMP}} \equiv (1/L_{\delta B_+} + 1/L_{\delta B_-}) \sim 2k_\theta$ and $\mathrm{w}_{\mathrm{pol}} \simeq (1.3\text{–}1.9)\ \mathrm{w}_{\mathrm{ib}} \simeq (3.7\text{–}5.4)$ cm represents [10] polarization current effects due to the finite ion banana width $\mathrm{w}_{\mathrm{ib}} \equiv q\rho_i/\sqrt{\varepsilon} \simeq 2.9$ cm. When RMPs are small, $\mathrm{w}_{\mathrm{pol}}$ stabilizing effects cause $\delta\mathrm{B}_\theta$ and hence the island width to decay [see gray line in Fig. 3(c)]. However, if $\mathrm{w}_{\mathrm{vac}}$ is large enough so $\mathrm{w}_{\mathrm{vac}} > \mathrm{w}_{\mathrm{pol}}/(2m)^{1/3} \sim 1.3\text{–}1.9$ cm, RMP effects dominate in Eq. (1) and the 8/2 island grows**, as shown in Fig. 3(c) since $\mathrm{w} \propto (\delta\mathrm{B}_\theta)^{1/2}$. This island width is predicted to grow as $\mathrm{w} \sim \mathrm{w}_{\mathrm{vac}}(t/\tau_\mathrm{w})^{1/3}$ [i.e., $B_{mn} \propto (t/\tau_\mathrm{w})^{2/3}$]

in which the minimum $\tau_w \gtrsim w_{vac}/(3D_\eta \Delta'_{RMP}) \sim 3$ ms. This is reasonably consistent with the approximate doubling** of the HFS measured δB_θ from about 4715 to 4720 ms in Fig. 3(c). The nonlinear saturated island width can be predicted by balancing the first two terms in Eq. (1): $w_{sat} \simeq w_{vac} |\Delta'_{RMP}/\Delta'_{8/2}|^{1/2} \sim w_{vac} \propto B_{mn}(\rho_{8/2})^{1/2}$, which is perhaps fortuitously in reasonable agreement with the linear M3D-C1 modeling results in Fig. 2 where $B_{82}(\rho_{8/2})/B^{vac}_{mn}(\rho_{8/2}) \simeq 0.8$.

RMP-induced flutter transport: The flutter model is relevant because T_e is not constant on island flux surfaces since $\lambda_{e\,eff} < L_{island}$ [10]. When RMPs are applied, they induce [14] ambipolar n_e and T_e flutter diffusivities of order $D_{et} \propto B^2_{mn}$ and $\chi_{et} \lesssim 3D_{et}$. Estimates of D_{et} increase from 0.4 m^2/s at $\rho_{mid} \simeq 0.95$ to 1 m^2/s at $\rho_{mid} \simeq 0.91$. These magnitudes and their increase moving inward are sufficient to significantly reduce the gradients in this pedestal top region ($0.9 < \rho < 0.96$), thereby apparently stabilizing P-B modes and producing the ELM suppression in Fig. 1. In the pedestal steep gradient region ($0.96 < \rho < 1$) where D_{et} is smaller, flutter transport would likely mostly produce density pump-out since there typically [17] the minimum $D_{eff} \sim 0.04$ m^2/s whereas the minimum $\chi_e \sim 0.3$ m^2/s. The temporal variations of $n_{e\,ped}$ and $T_{e\,ped}$ in Fig. 1 are thus qualitatively consistent with the B^2_{mn} dependence of flutter diffusivities.

Summary: Tokamak FMR theory [9] has been used to describe and quantify physical processes involved in various stages of RMP effects and an ELM crash response that lead to bifurcation into an ELM-suppressed state: 1) in the ELMing equilibrium, flow screening is strong with little magnetic reconnection; 2) the RMP at $q = 8/2$ penetrates via FMR induced by the ELM crash which locks the toroidal flow to the lab frame (like error field mode locking); 3) the ELM crash provides a 8/2 seed island (like NTMs) governed by the MRE; 4) then, if the total 8/2 RMP is large enough, the internal tearing-type (magnetic island) response and flow bifurcate; and 5) flutter transport significantly reduces pedestal top gradients, stabilizing P-B modes and thereby suppressing ELMs. This analysis is for discharge 158115 in DIII-D [1, 2]. More work is required to determine how universal this ELM-crash-induced ELM suppression scenario is and its potential utility in defining criteria for achieving ELM suppression with RMPs in ITER.

*This material is based upon work supported by the U.S. Department of Energy, Office of Science, Office of Fusion Energy Sciences under Award Numbers DE-FG02-92ER54139, DE-FG02-86ER53218, DE-AC02-09CH11466 and DE-FC02-04ER54698.

References

[1] C. Paz-Soldan et al., Phys. Rev. Lett. **114**, 105001 (2015).
[2] R. Nazikian et al., Phys. Rev. Lett. **114**, 105002 (2015).
[3] T.S. Hahm and R.M. Kulsrud, Phys. Fluids **28**, 2412 (1985).
[4] R. Fitzpatrick, Nucl. Fusion **33**, 1049 (1993).
[5] R. Fitzpatrick, Phys. Plasmas **5**, 3325 (1998).
[6] A.J. Cole and R. Fitzpatrick, Phys. Plasmas **13**, 032503 (2006).
[7] E. Nardon et al., Nucl. Fusion **50**, 034002 (2010).
[8] F.L. Waelbroeck et al., Nucl. Fusion **52**, 074004 (2012).
[9] J.D. Callen, C.C. Hegna, M.T. Beidler, "Forced magnetic reconnection in tokamak plasmas," to be published.
[10] J.D. Callen, N.M. Ferraro, C.C. Hegna, R.J. La Haye, R. Nazikian, C. Paz-Soldan, "Effects of resonant 3-D magnetic fields on pedestals," 15th Int.H-mode Wkshp.19-21 Oct. 2015, Garching, Germany, to be published.
[11] N.M. Ferraro, Phys. Plasmas **19**, 056105 (2012).
[12] C.C. Hegna, J.D. Callen and R.J. LaHaye, Phys. Plasmas **6**, 130 (1999).
[13] P.H. Rutherford, Phys. Fluids **16**, 1903 (1973).
[14] J.D. Callen, C.C. Hegna and A.J. Cole, Nucl. Fusion **53**, 113015 (2013).
[15] M.R. Wade et al., Phys. Plasmas **12**, 056120 (2005).
[16] A. Diallo et al., Phys. Plasmas **22**, 056111 (2015).
[17] J.D. Callen et al., Nucl. Fusion **50**, 064004 (2010).